Thin Solid Films 520 (2011) 1102–1108

Contents lists available at SciVerse ScienceDirect

Thin Solid Films

journal homepage: www.elsevier.com/locate/tsf

Structural morphology and magnetism of electroless-plated NiP films on a surface-modified Si substrate

Chun-Chao Huang, Hao-Chun Hsu, Yuan-Chieh Tseng *

Department of Materials Science & Engineering, National Chiao-Tung University, 1001 Ta Hsueh Road, Hsin-Chu, Taiwan 30010, Taiwan, ROC

ARTICLE INFO

Article history:
Received 4 March 2011
Received in revised form 6 September 2011
Accepted 13 September 2011
Available online 22 September 2011

Keywords:
Electroless-plating
Nickel–phosphorus alloy
Anisotropy
Structural morphology
Transmission electron microscopy
Atomic force microscopy
Magnetic properties

ABSTRACT

NiP thin films were deposited on an H_3PO_4-etched Si substrate by means of electroless-plating. By varying the plating time, we were able to deposit NiP films with various thicknesses. Thickness effects upon the structural morphology and magnetic properties of the NiP films were investigated, and they can be comprehended with a model of the deposition mechanism. The results demonstrate that the etched Si surface contained groove-like microstructure which shaped the columnar structure inside the NiP films and favored the film deposition; this was hard to achieve with a smooth-surfaced Si substrate. The well-developed columnar structure resulted in a perpendicular anisotropy due to its vertical nature, which can become superior to the film's longitudinal anisotropy if the applied field is sufficient.

1. Introduction

Excellent tribological properties have long been the trademark of electroless-plated NiP alloys. With its simplicity in operation, low cost, high corrosion and wear resistance, electroless-plated NiP has found wide application in enhancing the life of components exposed to severe conditions [1,2]. The study of electroless-plated NiP on Si substrates has been of particular importance in recent decades owing to its promising thermal and electrical properties which could extend its use from mechanical-coating to microelectronics and semiconductor industries [3–5], thereby greatly increasing its exposure in technologically advanced sectors. Researches concerning the (micro) structure, contact resistance, and junction characteristics of NiP/Si are, therefore, on the rise [6–8], as these factors are critical to the performance of the related devices. However, with all the research efforts devoted to the electrical and tribological properties, it has been easy to overlook other interesting characteristics inherent in NiP/Si; for example, its magnetic properties.

In the electroless-plating process, the driving force for the deposition of the NiP is supplied by a chemical reducing agent in the plating solution [9]. This driving potential is constant at all points of the surface and it enables a uniform concentration and thickness of the NiP over the substrate's landscape. As a consequence, modifying the substrate's surface configuration can somehow influence the subsequent deposition, thus leading to different structural morphologies for the NiP film. Since magnetism is quite sensitive to a material's structural configuration [10,11], the surface-modified substrate provides a platform for monitoring the effect of structural differences on the NiP's magnetic responses. As presented below, we established the interdependency between the structural morphology and the magnetic properties for the NiP/Si. This is to shed a light into the field which is still impoverished to date. We discovered that, with the NiP film, more than 500 nm could be deposited on an etching-modified Si substrate. The deposited films featured a columnar structure which was responsible for the film's unusual magnetic anisotropy.

2. Experimental details

The plating solution was composed of a mixture of $NiSO_4\,6H_2O$, $Na_2C_4H_4O_4\,6H_2O$, $NaH_2PO_2\,H_2O$, and $Pb(NO_3)_2$, which were the main nickel source, buffer agent, reducing agent, and stabilizing agent, respectively. The pH value and environmental temperature for the deposition were set to be 5.0 and 65 °C, respectively. Details about the plating solutions used in this work are listed in Table 1. A *p*-type Si substrate was etched by H_3PO_4 (86% as volume percentage) at ~50 °C. In order to understand the surface-roughness effect upon the magnetic properties of the NiP film, a plain (smooth), *p*-type Si substrate was also prepared for NiP deposition. Before the electroless-plating, the two kinds of Si substrates were sensitized by immersion in an $SnCl_2$/HCl solution for 2 min

* Corresponding author. Tel.: +886 3 573 1898; fax: +886 3 572 4727.
E-mail address: yctseng21@mail.nctu.edu.tw (Y.-C. Tseng).

0040-6090/$ – see front matter © 2011 Elsevier B.V. All rights reserved.
doi:10.1016/j.tsf.2011.09.025

Table 1
Bath compositions of the NiP electroless-plating process.

Compositions	Chemicals	Concentration
Sensitizer	$SnCl_2 + HCl$	40 g/l + 40 ml
Activator	$PdCl_2 + HCl$	0.14 g/l + 2.8 ml
Nickel source	$NiSO_4 \cdot 6H_2O$	20 g/l
Buffer agent	$Na_2C_4H_4O_4 \cdot 6H_2O$	16 g/l
Reducing agent	$NaH_2PO_2 \cdot H_2O$	27 g/l
Stabilizing agent	$Pb(NO_3)_2$	1 ppm

in order to form a uniform sensitization layer. Then the sensitized Si substrates were activated by immersion in a $PdCl_2$/HCl solution for 30 s. In the activation process, Pd^{+2} was chemically reduced to Pd, thus forming the nucleation center for the electroless-plating on the Si substrates, as discussed later. The surface morphologies of the etched Si and the smooth Si were probed by an atomic force microscope (AFM) for comparison. The AFM scanned area was $5 \times 5\ \mu m^2$ for all the samples. The NiP films were deposited by bathing the Si substrate in the plating solution over varying periods of time. Three NiP/Si samples with various thicknesses were investigated in this work. They were prepared by bathing the Si in the plating solution for 2, 6, and 10 min. The sizes of the Si substrates used for depositing the three samples were almost identical in order to isolate the thickness-dependent effects on the resulted properties.

All the samples were annealed at 400 °C for 2 min using a rapid thermal annealing facility to produce a ferromagnetic (FM) phase [12]. Sample thickness and cross-sectional morphology were verified using a scanning electron microscope (SEM, JSM 6500 F, operated at 15 kV). The sample surface morphology and roughness were probed by AFM (Veeco (ESCOPE-V), using a silicon tip operated at tapping mode with a frequency of 290–345 kHZ). The sample composition was determined by energy-dispersive X-ray spectrometry (EDX, JSM 6500F, working distance ~10 mm, life acquisition time ~60 s.) over several spots for each sample. A transmission electron microscope (TEM, JEM-2100F, operated at 200 kV) was used to probe the microstructure and atomic-scale images. The magnetic properties of the samples were identified using a vibrating sample magnetometer (VSM, VersaLab, manufactured by quantum design), which collected magnetic hysteresis (M-H) curves along the samples' in-plane (IP) and out-of-plane (OP) directions at 50 K and 300 K. We found that the Si substrate displayed a diamagnetic background. As detailed in the following, the VSM data shown in this paper all carefully excluded Si's contribution to ensure that the magnetic anisotropies observed in the samples were correctly presented. We measured the raw M-H curve (1st M-H) of the sample (NiP on Si), and then removed the NiP from the Si substrate by mechanical polishing. The remaining sample was examined by SEM to ensure the complete removal of the NiP, and then was sent to the VSM (2nd M-H) measurement again. We subtracted the 2nd M-H (only Si) from the 1st M-H (NiP on Si) to ensure that the magnetic properties were contributed from the NiP alone. We applied this method to both IP and OP considering that the Si's diamagnetic signal was axial-dependent. We also found that the variation in diamagnetic signal was insignificant between the smooth and the etched Si substrates.

3. Results and discussion

Fig. 1(a) and (b) shows the topographical images obtained in the *p*-type Si (100) substrate before and after H_3PO_4-etching, respectively. As suggested by the microscopy, the etched Si displays a rugged pattern with a surface roughness of ~35 nm. The roughness is estimated by averaging the highest and the lowest points over the probed area of the

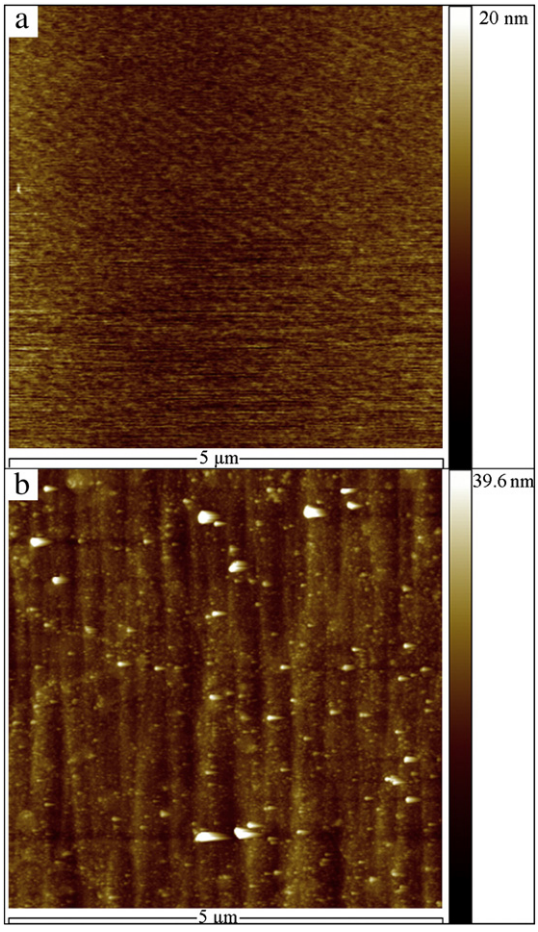

Fig. 1. AFM topographical images for a (a) smooth and a (b) H_3PO_4-etched Si substrate. X–Y plane defines the scanned area, and Z-axis scales the surface roughness.

etched substrate. The rugged surface can be characterized as having a groove-like microstructure, which features a larger surface area than that of the smooth Si. We believe that this microstructure stabilizes the Pd plating by taking advantage of its large surface area in the activation process [13]. This also facilitates the subsequent attachment of the NiP over the Pd particle's vicinity in electroless-plating, as discussed below. Fig. 2(a), (b) and (c) shows the cross-sectional SEM images for the NiP films, with plating times of 2, 6, and 10 min, respectively. The thickness of the NiP film can be increased systematically with increases in plating time, and the films are characterized with thicknesses of ~160, 420 and 550 nm for 2, 6 and 10 min, respectively. The SEM information also indicates a columnar structure developing concomitantly with the film deposition. Such a columnar can be confirmed by the transmission electron microscopic (TEM) image of the 160 nm sample, as highlighted in the inset of Fig. 2(a). The result is similar to the structure reported by Tsai et al. [13] with a smoothed Si, indicating that the columnar structure can be thought of as an inherent nature of the NiP/Si, regardless of the nature of the Si surface.

In principle, if the operation parameters of the electroless bath are kept unaltered, the deposition shouldn't stop at a given thickness. However, we found that on a smoothed Si, the NiP film gradually lost structural uniformity as the thickness exceeded ~170 nm and the film tended to peel off. In such case, the deposited NiP cannot be defined as a film. We compared the morphologies of the NiP deposited on the etched and smoothed Si in Fig. 3. Combing the information from

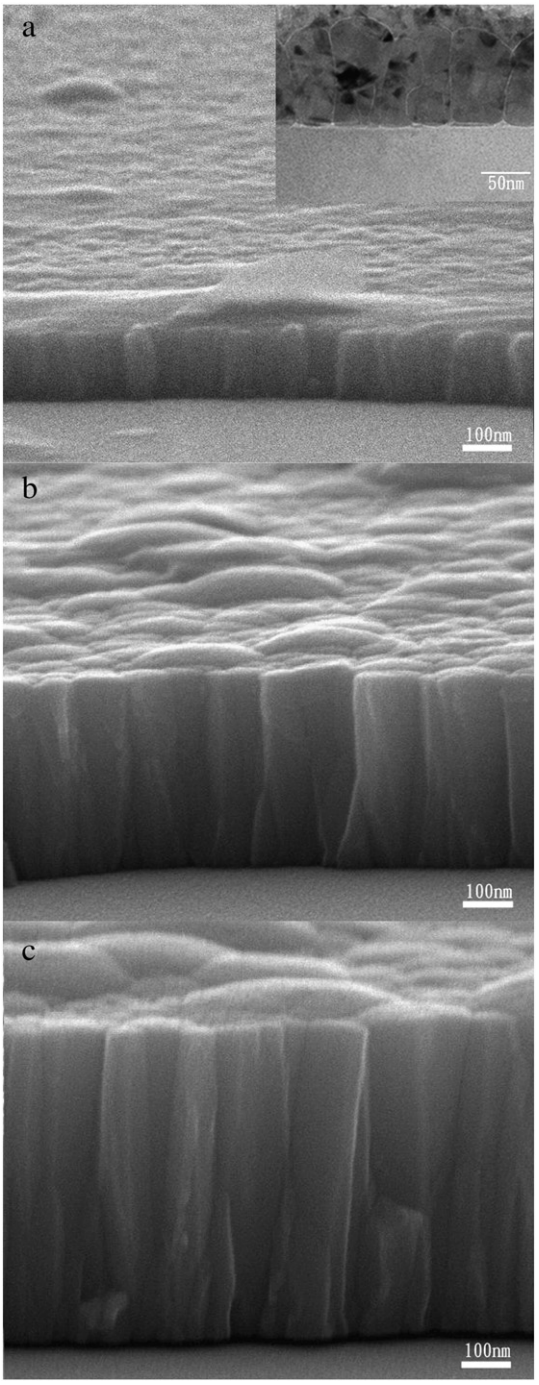

Fig. 2. SEM cross-sectional images for (a) 2-min plated, (b) 6-min plated and (c) 10-min plated NiP samples. Inset in (a) is the TEM cross-sectional view of the 2-min plated sample.

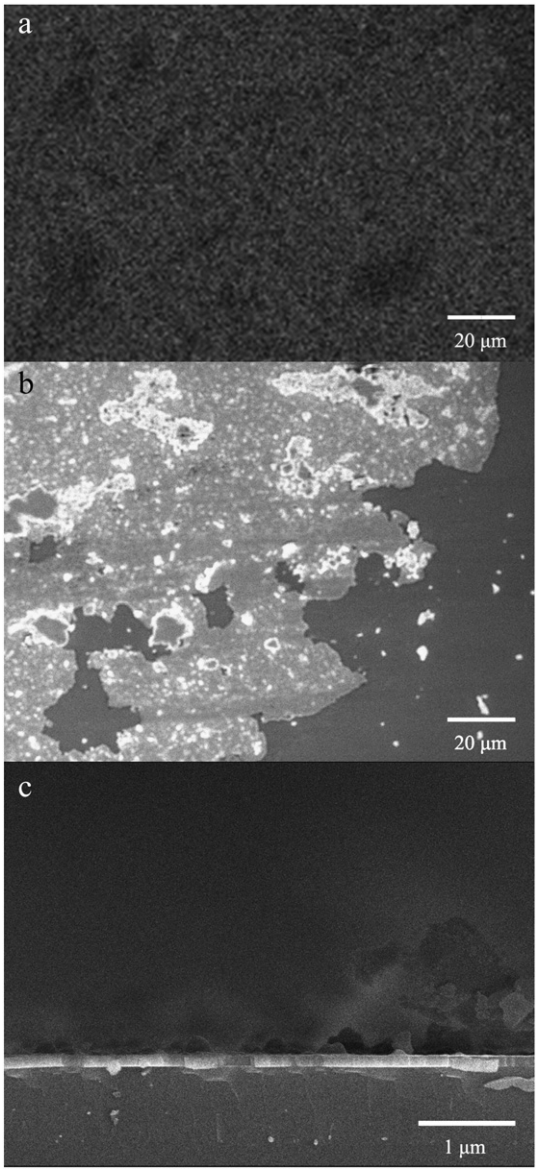

Fig. 3. (a) SEM top view for the NiP deposited on an etched Si substrate with a film thickness of ~160 nm. (b) and (c) are top view and cross-sectional images for the NiP deposited on a smoothed Si substrate, respectively, where the film thickness is ~170 nm. In (a), the lighter and darker regions are the NiP and Si, respectively. In (b), some irregular structures on top of the film can be seen in the right-hand side of the image, suggesting a less homogeneous structure than (a).

Figs. 2 and 3, it suggests that whether or not the NiP film can be uniformly increased to a certain thickness depends on the nature of the Si surface. Therefore, we provide a model (Fig. 4) similar to the one described in Ref. [13] to briefly interpret how the NiP developed the columnar structure on a surface-modified Si substrate. In the electroless-plating process, Pd ions serve as nucleation centers that allow the attaching of the Ni and P atoms through a chemical reducing reaction. The NiP first forms bunches, and accumulates continuously to deposit the film [13]. The groove-like microstructure (Fig. 1(b)) confines the initial expansion for the NiP bunches and prevents them from merging with each other, as illustrated in Fig. 4(a)–(d). The initial isolations within the bunches favor the growth of the columnar structure and shape its vertical nature as the deposition takes place, as illustrated in Fig. 4(e)–(g), which is supported by the increasing columnar structure observed in Fig. 2(a) to (c). The coalescing of the columnar structure on top determines the NiP's ultimate thickness. On the contrary, although a columnar structure is an inherent nature of the NiP, the smooth Si fails to strengthen the vertical nature for the columnar structure at early deposition due to the absence of the groove-like microstructure. This results in an early merging for the columnar structure which is responsible for the limited film thickness (Fig. 3). This implies that the etching-process for the Si is necessary for the depositing a robust NiP film. One may concern that the etched Si may possess higher

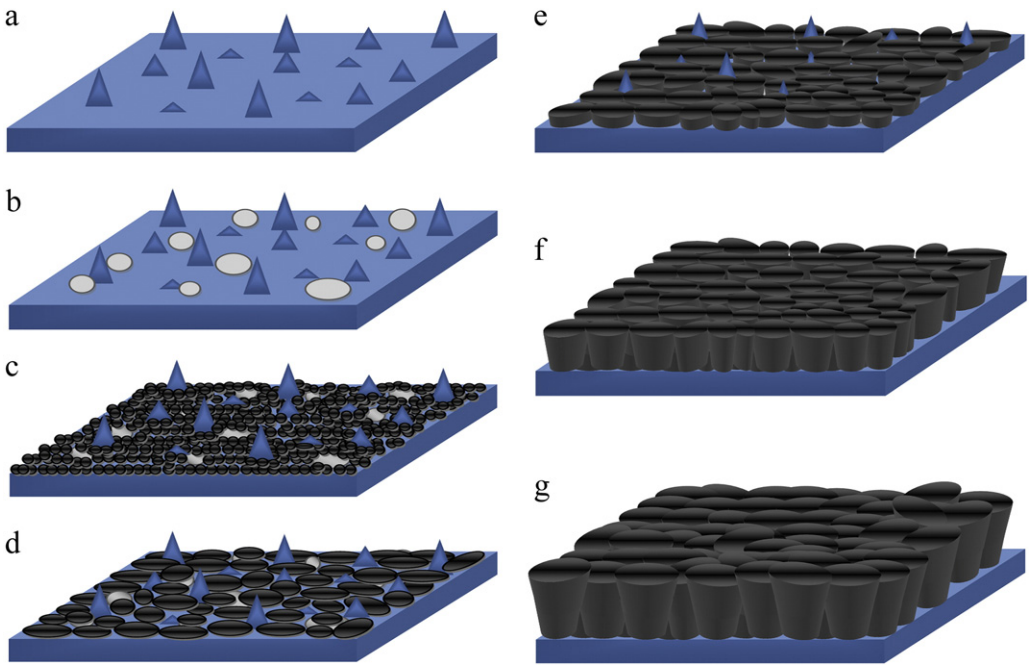

Fig. 4. Schematic illustration for the NiP deposition mechanism on a surface-modified Si substrate. (a) to (d) describe the nucleation of the NiP bunches and they are separated by the groove-like microstructure. (e) to (g) describe the growth of the columnar structure along with the film deposition.

energy surface than does the smooth Si, and that the surface diffusion/reaction effect may have taken place in the former case due to chemical instability, thus leading to a growth mechanism distinct from the proposed model (Fig. 4). However, the surface diffusion/reaction effect is neglected in our model as the NiP plating was done long after the Si was etched. The etched surface is chemically passivated before being plated with the NiP, and thus it influenced the NiP development in a very minor way. Furthermore, both the etched and the smooth Si were deposited with a thin activation layer before being plated, which would have reduced the surface energy difference between the two substrates even if the surface energy difference existed. In summary, we concluded that the NiP development was mainly governed by the surface geometry rather than the surface chemical instability. However, the groove-like microstructure only favors the deposition in a limited way. Its assistance is mainly effective at early deposition process due to its shallow roughness. For example, 550 nm is the largest achievable thickness using this method. A slower deposition rate after 400 nm is indicative of the gradually disappearing assistance delivered by the substrate.

We found that the columnar structure extends its characteristics to the top of the film and leads to various terminations depending on the film thickness. The terminations are characterized with granular structures, as shown in Fig. 5. The granular structure resulted from the merging of the columnar structure and reflects the development of the columnar structure, as depicted in Fig. 4(g). The topographical profiles, as shown in Fig. 5 indicated that the average sizes of the granular structures are ~20, 50 and 150 nm in diameter, for 160, 420 and 550 nm samples, respectively. From 420 to 550 nm, the sudden increase in granular size suggests that the columnar structure is developed remarkably in this period. Fig. 6 shows the topographical profile for the partially uniform region of the NiP with the smooth Si (Fig. 3). Clearly, the granular structure of the partially uniform NiP is less significant than the thinnest NiP with the etched Si (Fig. 5(a)), which suggests a weaker columnar structure resulting from the smooth substrate. In the scanned region some knob structures higher than 100 nm can be seen, which can be correlated to the irregularities observed in the SEM (Fig. 3(b), (c)). From the SEM (Fig. 3(b), (c)) and AFM (Fig. 6) of the NiP/smoothed Si, the partial suppression of the columnar structure seemed to result in the explosions of the NiP in other regions in order to balance the continuous deposition. The imbalanced deposition over the landscape of the smoothed Si therefore led to an inhomogeneous morphology (Fig. 3(b), (c)), making it different than the homogeneous NiP we observed in the etched Si (Figs. 2 and 3(a)).

Fig. 7(a), (b) and (c) presents the high resolution TEM (HRTEM) images of the 160, 420 and 550 nm samples with as-deposited condition, respectively. It is clear that all the samples exhibit nano-crystalline microstructure, where the nano-crystals (NC) feature an average diameter of ~3 nm and the samples are suggested to be superparamagnetic [12]. The NC size varies insignificantly from sample to sample, suggesting that it is independent of the development of the columnar structure. Nevertheless, the NC size here is slightly smaller than that reported in Ref. [13] (4–8 nm), probably due to the decrease in pH and the lower environmental temperature of the electroless bath. The micrographs of the three samples upon the RTA annealing are presented in (d), (e) and (f), with the same sample sequence as (a), (b) and (c). The results show that the crystallinity is enhanced by thermal annealing, whereas the enhanced NC sizes remain comparable (~8 nm) for the three samples. The enhanced microstructural ordering is responsible for the FM phases of the samples [12], as discussed in the following. Fig. 8(a) and (b) shows the M-H curves for the three samples measured along IP and OP at 50 K, respectively. The insets of Fig. 8(a) and (b) show the zoom-in information for IP and OP M-H curves at low field, respectively. As expected, the magnetization increases with the film thickness for both IP and OP because of the increase in Ni content. However, there is a significant increase in magnetization from 420 nm to 550 nm. The magnetization increasing factor (~3) is larger than the thickness increasing factor (~1.3), making it hard to conclude the phenomenon to be solely thickness-dependent. The EDX analysis, as

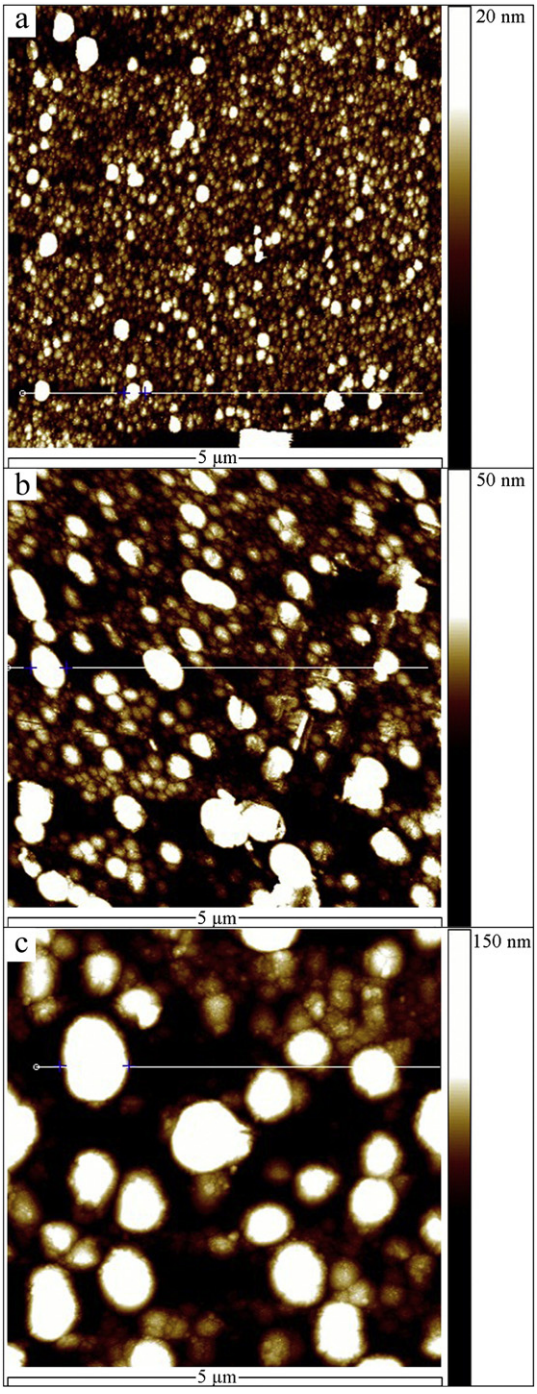

Fig. 5. Two-dimensional AFM topographical images for the (a) 160 nm, (b) 420 nm and (c) 550 nm NiP samples. Brighter regions indicate spots with higher altitudes. The AFM scanned area was $5\times5\ \mu m^2$ for all the samples.

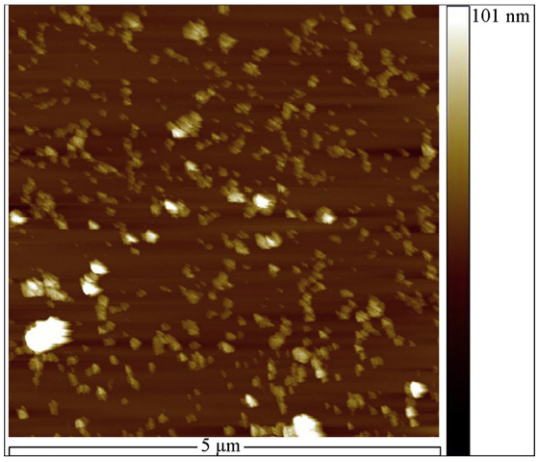

Fig. 6. AFM topographical image for a partially uniform region of a ~170 nm NiP film deposited on a smooth Si substrate.

shown in Table 2, reveals that the Ni (P) atomic percentage varies in a minor way (<3%) among the three samples. Although the minor variation in phosphorous content may be able to influence the grain size [13–15], from our TEM results (Fig. 7) it shows that such influence is not significant. This may be attributed to the EDX analysis used in this work, whose fluorescence background usually yields a probing deviation of 5–6%, but the true phosphorous contents of the three samples may be in a very close proximity so that the change of the NC size is not evident in our case. The comparable Ni contents for the three samples rule out the possibility that the unusual increase/decrease in the Ni percentages among the samples may have directly influenced the magnitude of FM ordering. Besides, since the NC size is independent of the NiP thickness, it suggests that the morphology plays a more important role in determining the magnetic ordering.

We correlate the enhanced magnetic ordering with the well-developed columnar structure in the 550 nm sample (Fig. 2(c)). It is reported by C. M. Liu et al. [12] that the microstructure (crystallinity) and the magnetism are strongly coupled for the NiP. This phenomenon is interpreted as a magneto-structural correlation, meaning that an increase in the structural ordering can enhance the FM ordering. In conjunction with Fig. 4, since the columnar structure developed significantly from 420 to 550 nm, a stronger FM ordering is expected to emerge in this period, leading to the much enhanced magnetization we observed macroscopically.

The insets of Fig. 8 show that the coercive field (H_c) is independent of thickness for both IP and OP. This indicates that the magnetic hardness varied little as the film becomes thicker. For all the samples, saturation magnetization is found in IP with an applied field greater than 5000 Oe. However, all the samples are hard to reach saturation with the same field in OP, especially the 550 nm sample. This suggests that IP is the magnetic easy-axis, which is consistent with the longitudinal anisotropy commonly seen in magnetic thin-film structures [16–20]. Fig. 9(a) highlights the three samples' absolute magnetizations collected at 1 T for IP (filled circles) and OP (open circles). Fig. 9(b) presents the same information with an applied field of 2 T. Two additional samples with plating times of 4 and 8 min, together with the 300 K data (squares) of all the samples, were added to Fig. 9 to confirm the trend. Interestingly, in Fig. 9(a), IP and OP exhibit close magnetizations for 160 and 420 nm, while OP's magnetization becomes superior to IP's as the film reaches 550 nm. Since the magnetization value reflects the magnetizing effect of a material under a magnetic field, the data reveal a thickness-dependent anisotropy, where the magnetization becomes more effective in OP as the film becomes thicker. Such phenomenon is even more significant when the field strength is doubled (Fig. 9(b)). The conclusion is supported by the 300 K data in both 1 and 2 T conditions, as the trend follows the same route even if the samples covered a large temperature range. The unusual magnetic anisotropy is attributed to the columnar structure, whose vertical nature can be thought of as the origin of the perpendicular anisotropy. Such perpendicular anisotropy is microscopic and negligible as the film is thin (160 and 420 nm). However, it is able to compete with the macroscopic, longitudinal

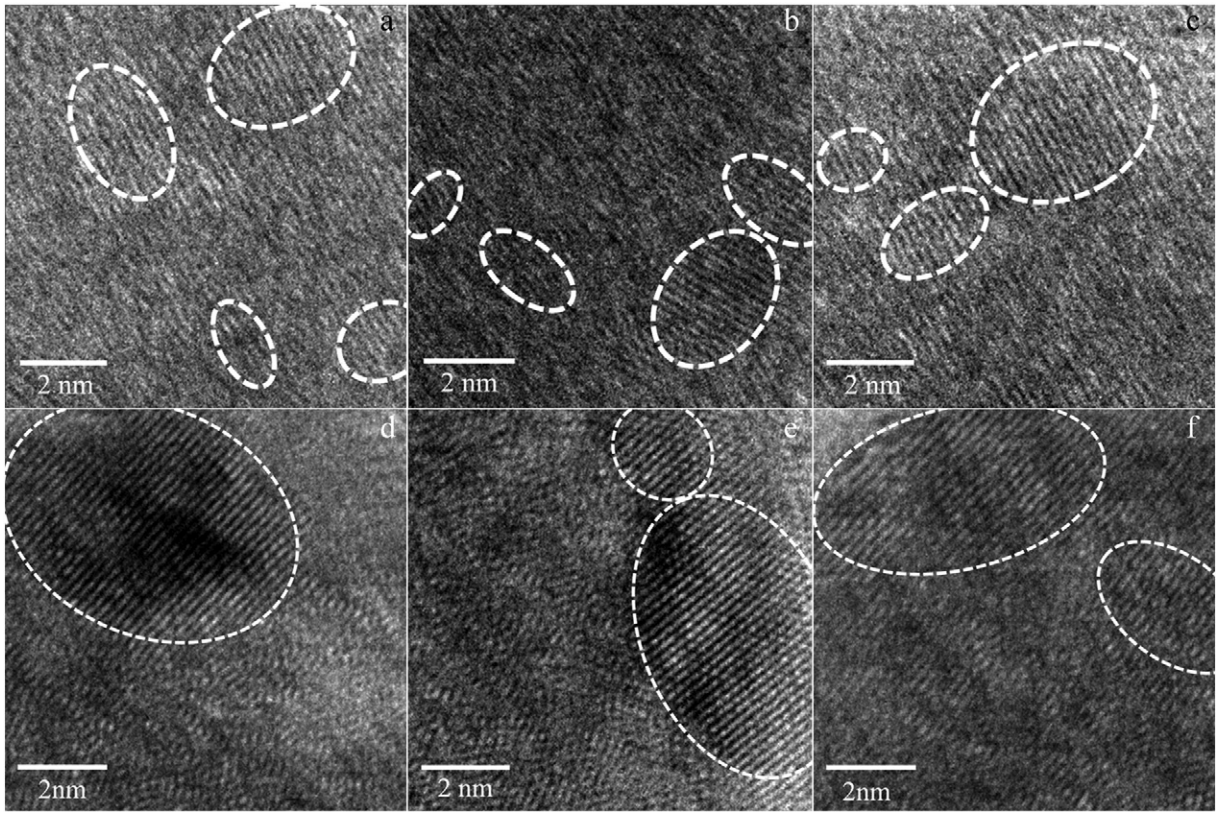

Fig. 7. HRTEM images for the (a) 160 nm, (b) 420 nm and (c) 550 nm NiP samples with as-deposited condition. (d), (e) and (f) are the images for the same sample sequence but with post-annealing condition. Dashed circles highlight the nano-crysalline structures of the samples.

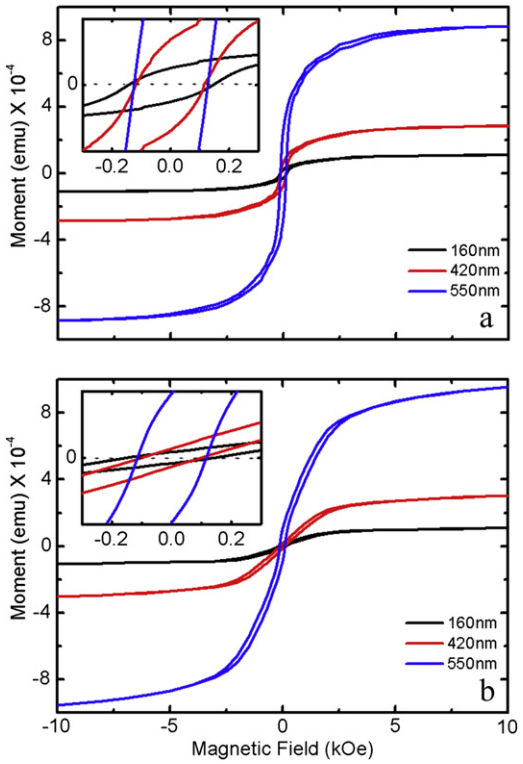

Fig. 8. Magnetic hysteresis (M-H) curves for the three samples for (a) in-plane (IP) and (b) out-of-plane (OP) measurements. Data were taken at 50 K. Insets for (a) and (b) are the zoom-in information for IP and OP M-H curves at low field, respectively.

Table 2
EDX compositional analysis for the NiP with various plating times.

Samples	Ni (atomic %)	P (atomic %)
2 min	81.6	18.4
6 min	84.0	16.0
10 min	84.0	16.0

shape anisotropy when the columnar structure is well developed (550 nm) and the magnetic field is high (2 T).

4. Conclusion

In summary, this work has reported on an investigation of the interplay between the structural morphology and magnetic properties of electroless-plated NiP thin films on an Si substrate. By bathing an etched Si substrate in the plating solution for sufficient time, we were able to deposit the film to 550 nm thick. The columnar structure was found to develop as the film thickness increased, leading to a microscopic, perpendicular anisotropy against the macroscopic longitudinal anisotropy.

Acknowledgements

The authors thank Mr. Chien-Yi Lee for kind help with the AFM data collection. The work is supported by the National Science Council of Taiwan under Grant No. NSC 98-2112-M-009 022-MY3.

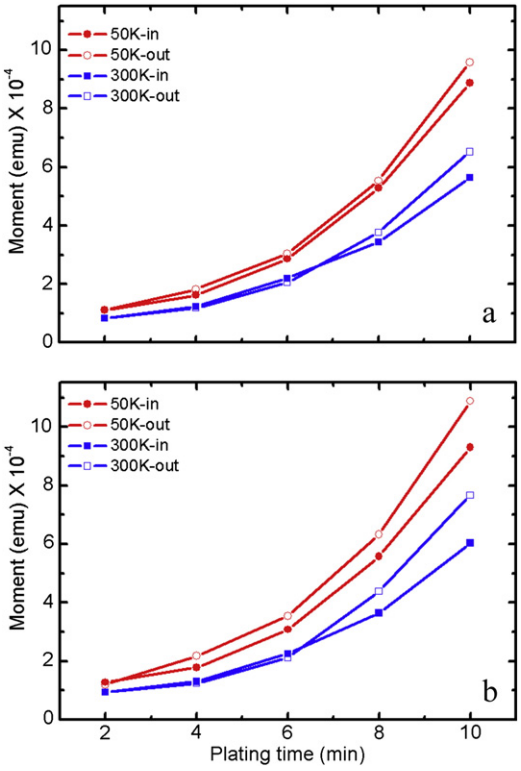

Fig. 9. Magnetization as a function of sample plating time for IP (filled symbols) and OP (open symbols) measurements, taken at 50 (circles) and 300 K (squares), taken at (a) 1 T and (b) 2 T.

References

[1] I. Apachitei, J. Duszczyk, Surf. Coat. Technol. 132 (2000) 89.
[2] M. Crobu, A. Scorciapino, B. Elsener, A. Rossi, Electrochim. Acta 53 (2008) 3364.
[3] B.K. Crone, A. Dodabalapur, R. Sarpeshkar, R.W. Filas, Y.Y. Lin, Z. Bao, J.H. O'Neill, W. Li, H.E. Katz, J. Appl. Phys. 89 (2001) 5125.
[4] H. Ashassi-Sorkhabi, S.H. Rafizadeh, Surf. Coat. Technol. 176 (2004) 318.
[5] V.M. Dubin, S.D. Lopatin, V.G. Sokolov, Thin Solid Films 226 (1993) 94.
[6] S. Dhar, S. Chakrabarti, Appl. Phys. Lett. 68 (1996) 1392.
[7] H. Iwasa, M. Yokozawa, I. Teramoto, J. Electrochem. Sci. 115 (1968) 485.
[8] C.M. Liu, W.L. Liu, S.H. Hsieh, T.K. Tsai, W.J. Chen, Appl. Surf. Sci. 243 (2005) 259.
[9] L.M. Abrantes, J.P. Correia, J. Electrochem. Sci. 141 (1994) 2356.
[10] H. Li, H.Z. Wu, G.X. Xiao, Powder Technol. 198 (2010) 157.
[11] J.M. Wesselinowa, J. Magn. Magn. Mater. 322 (2010) 234.
[12] C.M. Liu, Y.C. Tseng, C. Chen, M.C. Hsu, T.Y. Chao, Y.T. Cheng, Nanotechnology 20 (2009) 415703.
[13] T.K. Tsai, C.G. Chao, Appl. Surf. Sci. 233 (2004) 180.
[14] G. McMAhon, U. Erb, J. Mater. Sci. Lett. 8 (1989) 865.
[15] U. Erb, Can. Metall. Q. 34 (1995) 275.
[16] C. Nacereddine, A. Layadi, A. Guittoum, S.-M. Ch´erif, T. Chauveau, D. Billet, J. Ben Youssef, A. Bourzami, M.-H. Bourahli, Mater. Sci. Eng. B 136 (2007) 197.
[17] X. Zhou, F. Lin, X. Ma, W. Shi, J. Magn. Magn. Mater. 320 (2008) 1817.
[18] S.-M. Che´rif, A. Layadi, J.B. Youssef, C. Nacereddine, Y. Roussigne, Physica B 387 (2007) 281.
[19] R. Gupta, K.P. Lieb, G.A. Müller, M. Weisheit, K. Zhang, Nucl. Instrum. Methods Phys. Res. B 246 (2006) 393.
[20] H.M. Du, P. Wu, E.Y. Jiang, Z.Q. Li, C. Zhao, H.L. Bai, J. Magn. Magn. Mater. 292 (2005) 227.